



Jangid, K., Gupta, R., Sahu, R. P., Zhitomirsky, I. and Puri, I. K. (2022) Influence of conductive porous electrodes on the apparent electrode kinetics of fenitrothion. *Journal of Electroanalytical Chemistry*, 910, 116200. (doi: [10.1016/j.jelechem.2022.116200](https://doi.org/10.1016/j.jelechem.2022.116200))

There may be differences between this version and the published version. You are advised to consult the published version if you wish to cite from it.

<http://eprints.gla.ac.uk/268179/>

Deposited on 30 March 2022

Enlighten – Research publications by members of the University of Glasgow
<http://eprints.gla.ac.uk>

Influence of Conductive Porous Electrodes on the Apparent Electrode Kinetics of Fenitrothion

*Krishna Jangid*¹, *Rohit Gupta*², *Rakesh P. Sahu*^{2,3}, *Igor Zhitomirsky*³, and *Ishwar K. Puri*^{1,2,3,4*}

¹Department of Engineering Physics, McMaster University, Hamilton, Ontario, Canada.

²Department of Mechanical Engineering, McMaster University, Hamilton, Ontario, Canada.

³Department of Materials Science and Engineering, McMaster University, Hamilton, Ontario, Canada.

⁴Department of Aerospace and Mechanical Engineering, University of Southern California, Los Angeles, California, USA.

AUTHOR INFORMATION

***Corresponding author**

McMaster University

1280 Main St. W.

Hamilton, ON L8S 4L7, Canada

Email: ikpuri@mcmaster.ca

ABSTRACT

Planar bare electrodes fabricated with surface-modified multiwalled carbon nanotubes (MWCNT) are used to detect organophosphate (OP) compounds, which are used as herbicides and fungicides but are harmful to human health. Deposition of carbon nanotubes on the surfaces of bare electrodes enhances electrocatalysis, increasing the electrode to analyte current response and narrowing peak-to-peak potential separation during cyclic voltammetry (CV). We hypothesize that, as the thickness of the deposited MWCNT layer decreases, FT mass transport between the layers of porous multiwalled carbon nanotubes changes from semi-infinite to thin-layer diffusion. This influences the electrode electrochemical response to the analyte. Using simulations and experiments, we show that when porous MWCNT are deposited on a conductive glassy carbon electrode the mass transport of fenitrothion (FT, an OP) changes from semi-infinite to thin-layer diffusion during CV. This alters the electrochemical response of the electrode and reduces peak-to-peak potential separation. To simulate CV response to FT, both the semi-infinite and thin-layer diffusion models are employed for the planar bare and modified porous surface electrodes. The transition from thin layer to semi-infinite diffusion is clear when the nanotube layer thickness on the bare electrode increases. The model is applicable to other toxic chemicals, such as 4-nitrophenol, parathion, or methyl parathion that have similar electrode kinetics.

KEYWORDS: Fenitrothion – Organophosphate – Cyclic voltammetry – Carbon nanotube – Thin-layer diffusion – Porous electrode – Heterogenous rate constant

1. Introduction

Organophosphorus (OP) compounds are widely used to improve agricultural production, contributing to 70% of pesticide consumption in agriculture.¹ The OP residue that persists in the environment has a serious public health impact, since it can lead to mental disorder, coma and death.² Due to human poisoning and associated illnesses from OP, an annual economic cost of \$1 billion is estimated in the U.S. alone.³ The typical analytical techniques to monitor OP include mass spectrometry⁴ and liquid or gas chromatography,⁵ but these require complex sample processing, skilled professionals, and are costly.⁶ Due to their lower cost, rapid response and high sensitivity, electroanalytical methods have emerged as promising methods for OP monitoring.

To lower the detection limit and improve sensor sensitivity, the electrochemical response of an electrode to an analyte must be enhanced. When nanomaterials, such as carbon nanotubes (CNT), are deposited on a bare electrode, the electrode specific surface area and electrical conductivity also increase,^{7, 8} which improves sensitivity by augmenting electrocatalysis,⁹ enhancing OP detection.^{7, 10, 11, 12} These faster electrode kinetics have been interpreted through the peak-to-peak potential separation of cyclic voltammograms, a comparison is valid when the mass transport of the analyte towards the electrode is the same for both the bare and modified electrode.⁹ However, the mass transport regime is not the same in both cases, making the argument in favor of faster electrode kinetics influenced by a CNT-modified electrode questionable.

The additional mass transport of analytes on the surfaces of CNT-modified electrodes occurs through thin-layer diffusion in contrast to semi-infinite diffusion for bare electrodes.^{9, 13-15} Semi-infinite diffusion of the analyte from the bulk solution occurs at the planar surface of the electrode, while thin-layer diffusion occurs between the layers of nanotubes containing trapped portions of the solution, as depicted in Fig. 1. Both the semi-infinite and thin-layer diffusion

models for ferrocyanide demonstrate that the thin-layer model produces a smaller peak-to-peak potential separation in cyclic voltammogram for a porous CNT/glassy carbon electrode (GCE) as compared to an unmodified GCE.⁹ Further evidence for thin-layer effects at the surface of a porous MWCNT/GCE electrode has been provided based on semi-infinite and thin-layer diffusion mixed mass transport for nicotine.¹³ Therefore, mass transport effects must be considered while explaining the electrochemical response of a porous modified electrode towards an analyte.

To simulate a cyclic voltammetry (CV) response, we select fenitrothion (FT) as the OP that undergoes multi-step and multi-electron electrochemical reactions. FT has a redox-active $-\text{NO}_2$ group that undergoes multi-step multi-electron electrochemical reactions, as shown in Fig. 2 (B). Application of a negative cathodic potential of $-0.6 \text{ V vs. Ag/AgCl}$ during cyclic voltammetry reduces the $-\text{NO}_2$ group of FT irreversibly to $-\text{NHOH}$ producing FT^{red} ¹² as shown in Fig. 7 (A). During subsequent scans, the $-\text{NHOH}$ and $-\text{NO}$ groups undergo quasi-reversible oxidation and reduction, forming FT^{ox} and FT^{red} , respectively. We are unaware of the existence of a theoretical model to simulate such multi-step and multi-electron electrochemical reactions like, FT.

Our objective is to simulate FT's electrochemical response at bare and porous modified electrodes to investigate the occurrence of thin-layer effects. We hypothesize that the change in the FT mass transport regime between the layers of porous multiwalled carbon nanotubes from semi-infinite to thin-layer diffusion influences the electrode electrochemical response to the analyte. This thin-layer effect lowers peak-to-peak potential separation during CV with a MWCNT/GCE compared to a bare GCE. We simulate the FT electrode kinetics at the surfaces of bare and porous modified electrodes to characterize the effects that arise due to thin-layer diffusion through the porous MWCNT deposit. The theoretical model should apply to other toxic

compounds with similar electrode kinetics, like 4-nitrophenol, parathion, or methyl parathion, that are typically used to synthesize pesticides, pharmaceuticals, and dyes.^{7, 16}

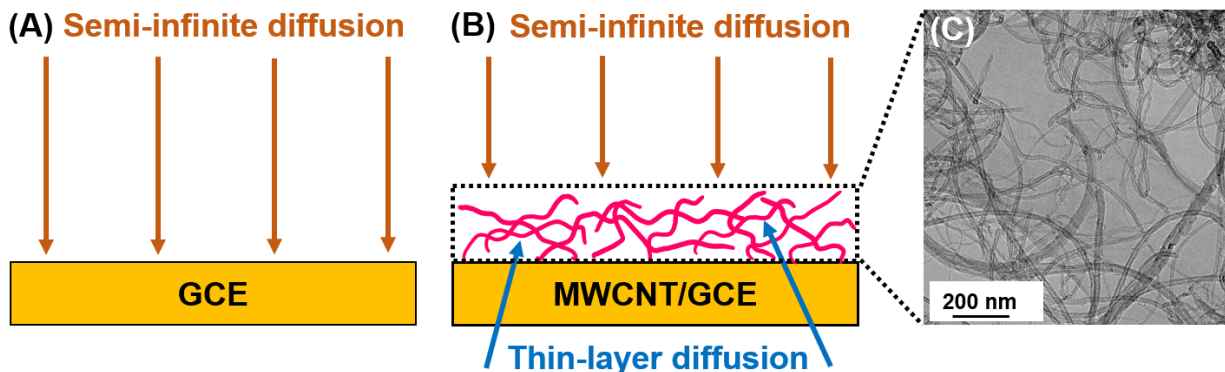


Figure 1. Schematics of the two different mass transport regimes present at the surfaces of (A) a glassy carbon electrode (GCE) and (B) a multiwalled carbon nanotube/glassy carbon electrode (MWCNT/GCE). (C) TEM image of the MWCNT.

2. Mathematical formulation

The CV responses to FT at the surfaces of the unmodified planar GCE and porous MWCNT/GCE are simulated using semi-infinite diffusion and thin-layer cell models.⁹ In contrast to the semi-infinite planar diffusion model, the thin-layer cell model contains both planar conductive and insulating layers.⁹ The solution containing the electroactive species is confined within these thin-layer cells, representing pockets of solution contained between MWCNT layers. The FT electrochemical reactions occur when electron transfer between FT and the electrode is thermodynamically and kinetically favorable, which generates redox peaks in the CV profiles.

We assume an idealized scenario, where only FT is present in the solution exposed to the electrodes. The starting, vertex and ending potentials used in the simulation are -0.2, -0.8 and 0.5 V, respectively. Table 1 contains a list of the dimensionless variables used to simulate the electrochemical process.

Table 1: List of all the dimensionless variable used for simulating the electrochemical reaction kinetics of the FT, where c_{FT} , $c_{\text{FT}}^{\text{red}}$, and $c_{\text{FT}}^{\text{ox}}$ denote the concentrations of FT, reduced FT, and oxidized FT, respectively. c_b initial bulk concentration of FT, ϵ radius of the macroscale disc electrode, A area of the electrode, x perpendicular coordinate from the electrode, R universal gas constant, T absolute temperature, F Faraday's constant, E imposed electrode potential, E_1^0 apparent formal potential for step A (see Fig. 2 (B)), $E_{\text{rds}}^{0'}$ and $E_{\text{non-rds}}^{0'}$ formal potentials for the second and first electron transfers of step B, $\Delta E^{0'} = E_{\text{rds}}^{0'} - E_{\text{non-rds}}^{0'}$, D diffusion coefficient of the species ($D = 6.9 \times 10^{-6} \text{ cm}^2 \text{ s}^{-1}$), t time, k_1^0 and k_2^0 apparent standard heterogeneous rate constants for step A and B (see Fig. 2 (B)), respectively, v scan rate, and i current.

Dimensionless quantity	Expressions
Concentration	$C_{\text{FT}} = \frac{c_{\text{FT}}}{c_b}$, $C_{\text{FT}}^{\text{red}} = \frac{c_{\text{FT}}^{\text{red}}}{c_b}$, and $C_{\text{FT}}^{\text{ox}} = \frac{c_{\text{FT}}^{\text{ox}}}{c_b}$
Distance	$X = \frac{x}{\epsilon}$
Potential	$\theta_1 = \frac{F(E-E_1^0)}{RT}$, $\theta_2 = \frac{F(E-E_{\text{rds}}^{0'})}{RT}$ and $\theta_{\Delta E^{0'}} = \frac{F\Delta E^{0'}}{RT}$
Rate constant for step A of reaction (see Fig. 2 (B))	$K_1^0 = \frac{k_1^0 \epsilon}{D}$
Rate constant for step B of reaction (see Fig. 2 (B))	$K_2^0 = \frac{k_2^0 \epsilon}{D}$
Time	$\tau = \frac{Dt}{\epsilon^2}$
Scan rate	$\sigma = \frac{F\epsilon^2 v}{RTD}$
Layer thickness	$L = \frac{\beta \sqrt{Dt_{\text{max}}}}{\epsilon}$
Current	$j = \frac{i\epsilon}{AFDc_b}$

The diffusion of electroactive species is represented through Fick's second law, and c_{FT} , c_{FT}^{red} , and c_{FT}^{ox} , are determined at the bare electrode and thin-layer cell by applying Eqs. (1)-(3). The diffusion coefficients for FT, FT^{red}, and FT^{ox} are assumed identical for sake of simplicity.

$$\frac{\partial C_{FT}}{\partial \tau} = \frac{\partial^2 C_{FT}}{\partial x^2}, \quad (1)$$

$$\frac{\partial C_{FT}^{red}}{\partial \tau} = \frac{\partial^2 C_{FT}^{red}}{\partial X^2}, \text{ and} \quad (2)$$

$$\frac{\partial C_{FT}^{ox}}{\partial \tau} = \frac{\partial^2 C_{FT}^{ox}}{\partial X^2}. \quad (3)$$

Two boundary conditions (at $X = 0$ and $X = L$ for $\tau > 0$) and an initial condition (at $0 \leq X < L$ for $\tau = 0$) are required to solve these equations. At the electrode surface ($X = 0$), the multi-electron, multi-step kinetics are governed by the IUPAC approved Butler-Volmer kinetic equation^{18, 19} (Eqs. (4)-(6)) which assumes that the second step of the irreversible reduction of FT to FT^{red} (i.e., step A) is the rate determining step (Fig. 3 A). This assumption is consistent with the behaviors of the experimentally measured cyclic voltammograms of bare and carbon nanotube modified electrodes. For the two-electron transfer reaction (step B), the second electron transfer is assumed to be the rate determining step (rds), while the first electron transfer remains in equilibrium (Fig. 3 B). Hence, kinetic equations guided by Bard & Faulkner²⁰ are derived, where $E_{rds}^{0'}$ and $E_{non-rds}^{0'}$ denote the formal potentials for the second and first electron transfers, respectively. In the bulk ($X = L$), the boundary condition differs for two scenarios, (a) pre-specified concentration of FT for semi-infinite diffusion and (b) no-flux boundary condition of the species (see Fig. 2 (A)) for thin layer diffusion. The $L \rightarrow \infty$ boundary condition is imposed at a reasonably large distance compared to the diffusion length scale $\sqrt{Dt_{max}}$ by introducing a multiplier $\beta = 2$.¹⁸ Further,

$$\left. \frac{\partial C_{FT}}{\partial X} \right|_{X=0} = K_1^0 \exp[-(1 + \alpha_1)\theta_1] C_{FT}, \quad (4)$$

$$\left. \frac{\partial C_{FT}^{red}}{\partial X} \right|_{X=0} = -K_1^0 \exp[-(1 + \alpha_1)\theta_1] C_{FT} + K_2^0 \exp[(1 - \alpha_2)\theta_2] C_{FT}^{red} - K_2^0 \exp(-\theta_{\Delta E^0'}) \exp[-(1 + \alpha_2)\theta_2] C_{FT}^{ox}, \text{ and} \quad (5)$$

$$\left. \frac{\partial C_{FT}^{ox}}{\partial X} \right|_{X=0} = -K_2^0 \exp[(1 - \alpha_2)\theta_2] C_{FT}^{red} + K_2^0 \exp(-\theta_{\Delta E^0'}) \exp[-(1 + \alpha_2)\theta_2] C_{FT}^{ox}. \quad (6)$$

Equations (1)-(3) coupled with Butler-Volmer electrode kinetic equations, Eqs. (4)-(6), are discretized using the finite volume method with equally spaced grid points. Time discretization is based on an implicit time scheme where current concentrations values at neighboring node are used for time marching. The resulting set of linear algebraic equations is cast in a classical tridiagonal matrix form and solved using the tridiagonal matrix algorithm (TDMA), which provides the one-dimensional spatiotemporal concentration for different species. All simulations are conducted in the MATLAB R2015a environment and run on a personal computer (Intel Core i7 processor @ 2.11 GHz, 16 GB RAM) for ≈ 2 seconds to generate each voltammogram. The MATLAB code is available at <https://github.com/Krishnajangid1996/Fenitrothion-electrode-kinetics>. Then, the overall electrochemical current response is calculated as follows,

$$j = -4 \frac{\partial C_{FT}}{\partial X} + 2 \frac{\partial C_{FT}^{ox}}{\partial X} \quad (7)$$

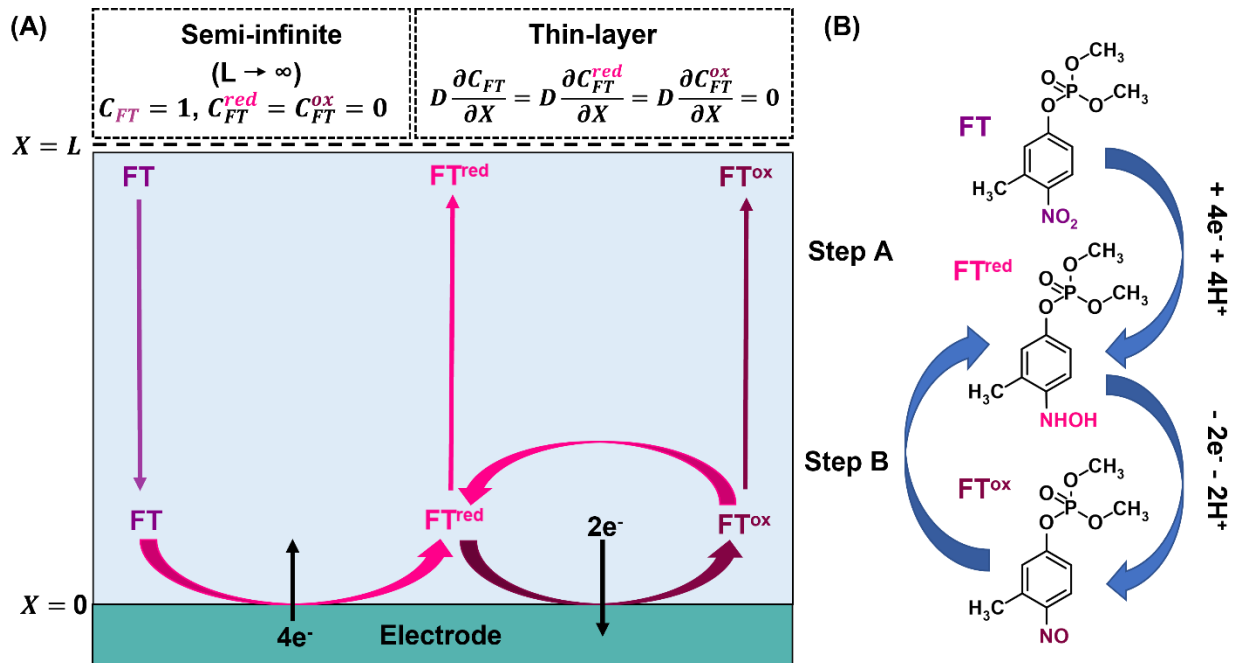


Figure 2. (A) Schematic of the boundary conditions for FT transport for the one-dimensional semi-infinite diffusion and thin-layer cell model where the species undergoes chemical reactions and produces electroactive species FT^{red} and FT^{ox}. (B) Schematic of the FT electrochemical reactions where the redox-active -NO₂ group produces electroactive FT^{red} and FT^{ox} through steps A and B.

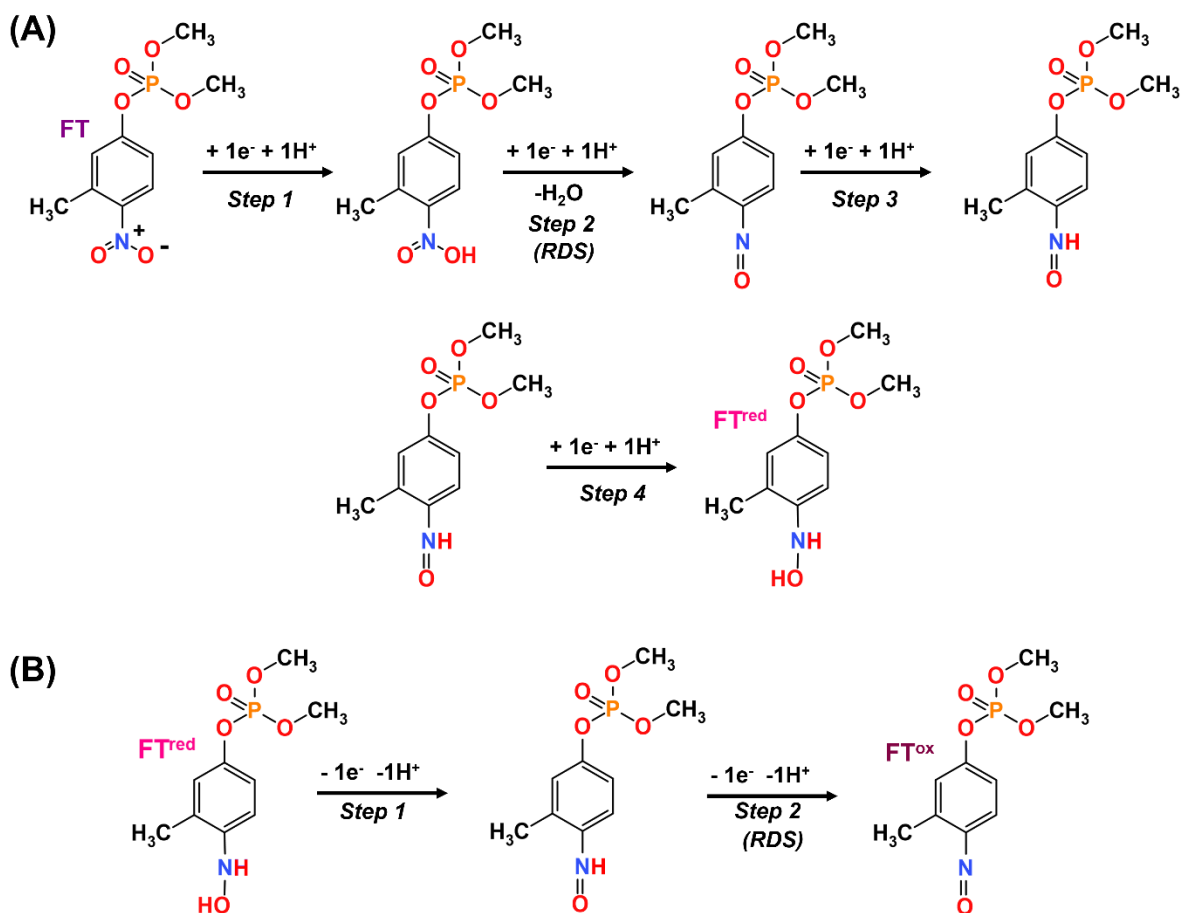


Figure 3. Schematics of the mechanism of (A) step A, and (B) step B of the FT electrochemical reactions producing electroactive FT^{red} and FT^{ox} .

3. Experimental

3.1. Chemicals and Instruments

Analytical grade FT and sodium acetate buffer solution (ABS) reagents were obtained from Sigma-Aldrich (USA). MWCNTs (length 1-2 μm , outside diameter 13 nm, and inside diameter 4 nm) were purchased from Bayer Inc. (Germany). Deionized water was used for all solution preparation. 0.1M NaOH and 0.1M HCl were used to adjust the pH of the buffer solution. FT stock solutions were prepared in ethanol and stored at 4°C. Electrochemical measurements were executed with a PARSTAT 2273 potentiostat, Princeton Applied Research, USA. A three-electrode arrangement

consisting of a GCE (bare working electrode), platinum wire (counter electrode) and Ag/AgCl (reference electrode) immersed in buffer solution was used for the cyclic voltammetric experiments. Transmission electron microscopy (TEM) characterization was performed with FEI Titan 80-300 LB instrument.

3.2. Preparation of MWCNT/GCE

MWCNTs were suspended in ethanol to form a 1 mg/mL suspension. Several volumes of the MWCNT suspension were drop casted on the GCE and dried in air to form MWCNT-modified GCEs. The electrochemical response of the electrodes was obtained by scanning them using cyclic voltammetry from -0.2 to -0.8 V, then -0.8 to 0.5V, followed by 0.5 to -0.2V. A 1 mM FT concentration and a 0.2 M ABS (pH 5) were used for all experiments. Scan rates of CV were varied from 50 to 175 mV/s.

4. Results and discussion

4.1. Theoretical results from the mechanistic model

The FT cyclic voltammetric simulations are performed and revealed the influence of thin-layer effects on the voltammetric response. Apparent standard rate constants for step A and B (Fig. 2 B) of FT at the bare planar and porous modified electrode are $k_{1,b}^0$, $k_{2,b}^0$ and $k_{1,m}^0$, $k_{2,m}^0$ respectively. We have assumed that rate constants of thin-layer diffusion model ($k_{1,m}^0 = 6.5 \cdot 10^{-2}$ cm/s, $k_{2,m}^0 = 8.2 \cdot 10^{-3}$ cm/s) are greater than the semi-infinite diffusion model ($k_{1,b}^0 = 4.2 \cdot 10^{-2}$ cm/s, $k_{2,b}^0 = 5.1 \cdot 10^{-3}$ cm/s). We first compare the peak-to-peak potential separation ΔE_{pp} for both semi-infinite diffusion and thin-layer diffusion models. Three different sets of rate constant values are considered, i.e., using (1) $k_{1,b}^0$, $k_{2,b}^0$ for semi-infinite diffusion and $k_{1,m}^0$, $k_{2,m}^0$ for thin-layer diffusion, (2) $k_{1,b}^0$ and $k_{2,b}^0$ for both models, and (3) $k_{1,m}^0$ and $k_{2,m}^0$ for both models. Hence, Case 1

uses different rate constants for semi-infinite and thin-layer diffusion, while Cases 2 and 3 use the same values for both models. For Case 1, ΔE_{pp} is lower for the thin-layer diffusion model than the semi-infinite diffusion model (Fig. 4 A). Use of the same rate constants for Cases 2 and 3 provides similar results (Figs. 4 B, C). Next, the experimental CVs of GCE (Fig. 6 A) and MWCNT/GCE (Fig. 6 E) are compared with the simulated CVs, where the kinetic parameters, including apparent standard heterogeneous rate constants, transfer coefficients and formal potentials $E_{rds}^{0'}$ and $E_{non-rds}^{0'}$, are varied to obtain similar peak current ratios (I_A/I_{C2} and I_{C1}/I_A), as shown in Figs. 5 A, B. Again, peak-to-peak potential separation ΔE_{pp} is lower for the thin-layer diffusion model than the semi-infinite diffusion model (Fig. 5 C). Considering the timescale of the experiments, when FT is considerably depleted in the thin-layer cell, less current is drawn,^{9, 13} which explains why ΔE_{pp} is lower for a thin layer.

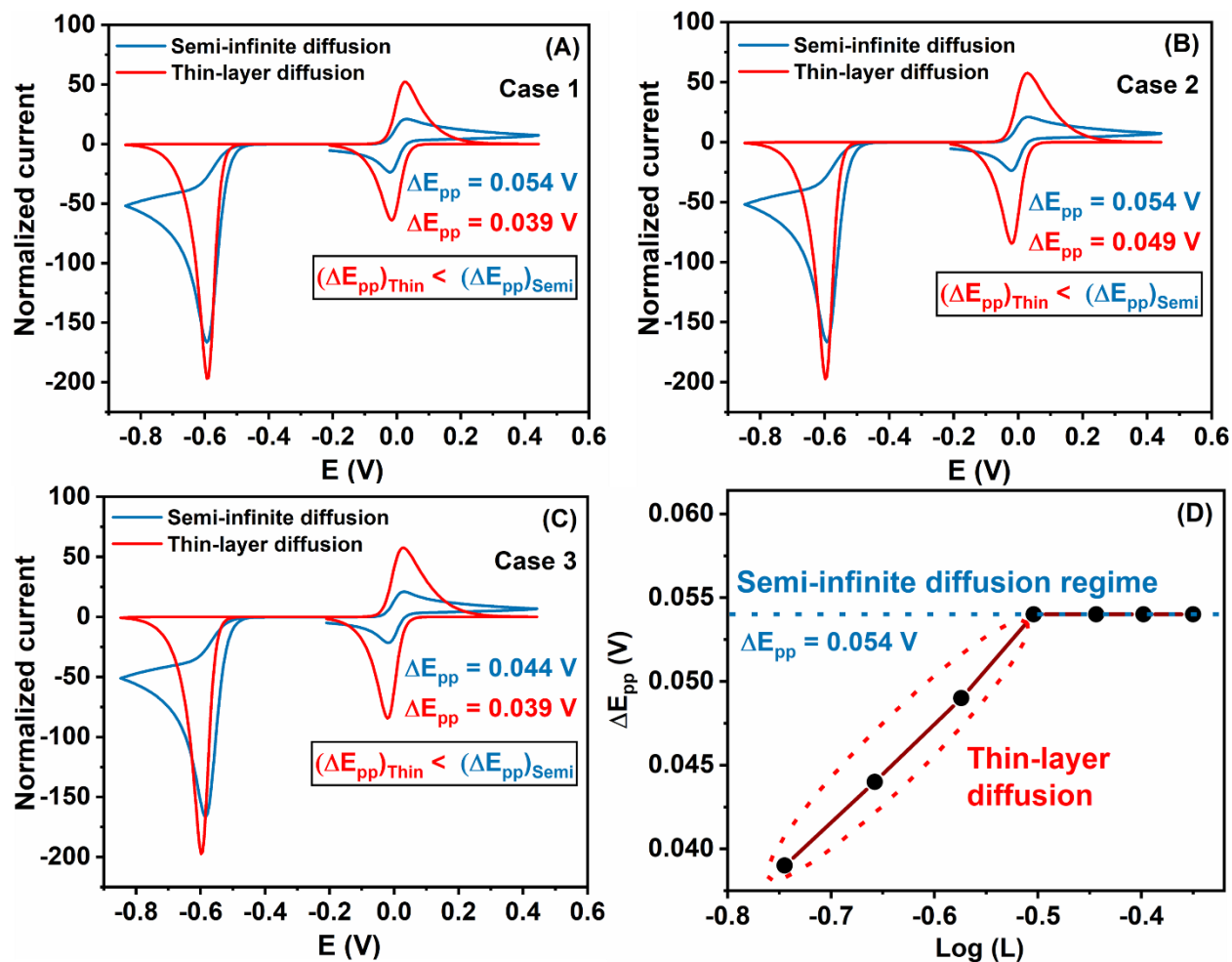


Figure 4. Simulated cyclic voltammograms for the semi-infinite and thin-layer diffusion models for (A) Case 1 that uses $k_{1,b}^0$, $k_{2,b}^0$ for the semi-infinite diffusion model and $k_{1,m}^0$, $k_{2,m}^0$ for the thin-layer diffusion model, (B) Case 2 using $k_{1,b}^0$ and $k_{2,b}^0$ for both models, and (C) Case 3 using $k_{1,m}^0$ and $k_{2,m}^0$ for both models, (D) Plot of peak-to-peak potential separation ΔE_{pp} vs. Log of the dimensionless layer thickness, L . The simulation parameters for all curves are $D = 6.9 \times 10^{-6} \text{ cm}^2 \text{ s}^{-1}$, $\nu = 0.1 \text{ V s}^{-1}$, $E_{rds}^{0'} = 5 \text{ mV}$, $E_{non-rds}^{0'} = 1 \text{ mV}$, and $C_b = 1 \text{ mM}$.

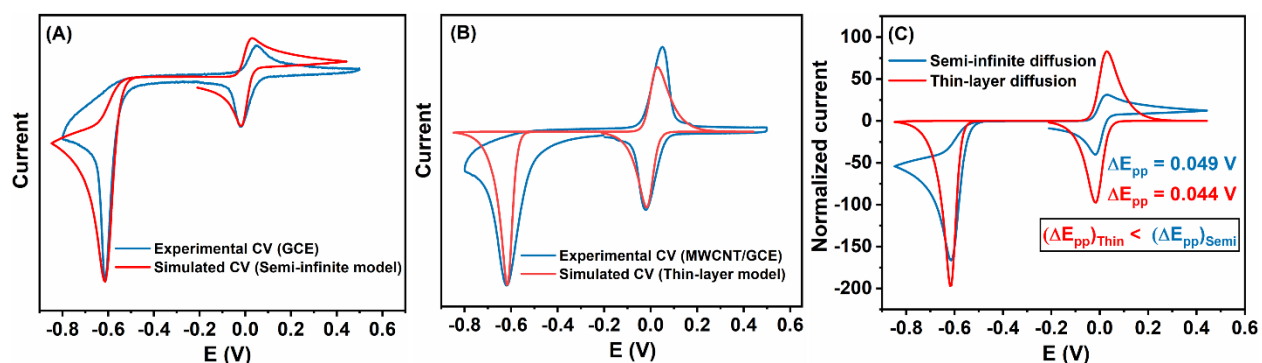


Figure 5. Superimposed plots of simulated and experimental CV of (A) GCE and (B) MWCNT/GCE. (C) Simulated cyclic voltammograms for the semi-infinite and thin-layer diffusion models for the experimentally matched CVs. The simulation parameters for all curves are $D = 6.9 \times 10^{-6} \text{ cm}^2 \text{ s}^{-1}$, $\nu = 0.1 \text{ V s}^{-1}$, $E_{rds}^{0'} = 7 \text{ mV}$, $E_{non-rds}^{0'} = 2 \text{ mV}$, and $C_b = 1 \text{ mM}$.

The FT response towards varying electrode surface characteristics is simulated for thin layers, where the dimensionless layer thickness L is varied and ΔE_{pp} for the simulated CVs plotted vs. $\text{Log}(L)$ (Fig. 4 D). All other parameters are identical to those used for Case 1. As shown in Fig. 4 D, with the increase in layer thickness, the peak-to-peak potential separation ΔE_{pp} increases since the diffusion layer is now larger.⁹ For sufficiently large layer thicknesses, ΔE_{pp} approaches the value simulated by the semi-infinite model. Since, the apparent standard heterogenous rate constants are held constant, changes in electrode geometry alter FT mass transport, changing ΔE_{pp} .

4.2. Results obtained from CV experiments

Cyclic voltammetry is routinely used with GCE and MWCNT/GCE to characterize mass transport changes. The dependence of peak current on scan rate shows whether the process involves semi-infinite (I vs. $\nu^{1/2}$) or thin-layer (I vs. ν) diffusion.¹⁴ Both cases are evaluated for all three voltammogram peaks (C_1 , A, and C_2) with the two electrodes. For the bare GCE (see Figs. 6 B, C and D), the peak current is linearly dependent on the square root of scan rate, confirming semi-infinite diffusion. For the MWCNT/GCE (Figs. 6 F, G and H), the peak current is instead linearly dependent on the scan rate itself, confirming thin-layer diffusion across the deposited nanotube interface on the GCE. Since FT transport across relatively small thin-layers is adsorption limited,¹⁴ the measurements are made immediately after MWCNT/GCE exposure to the solution, which minimizes FT adsorption.

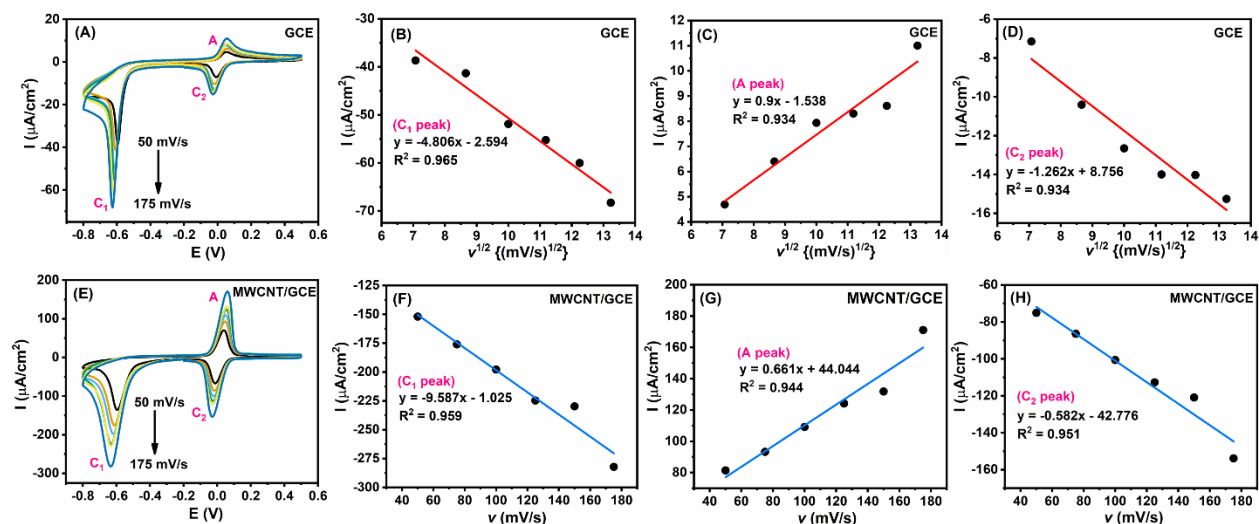


Figure 6. Cyclic voltammetry response of 1 mM FT in 0.2 M ABS (pH 5) at various scan rates ranging from 50 mV/s to 175 mV/s at (A) GCE and (E) MWCNT/GCE. Variation of peak current with respect to the square root of scan rate, I vs. $v^{1/2}$, for three different peaks (B) C_1 , (C) A, and (D) C_2 for 1 mM FT detection with a GCE. Plot of peak current vs. scan rate, I vs. v , for the (F) C_1 , (G) A, and (H) C_2 peaks when 1 mM FT is detected by an MWCNT/GCE. The background solution contains 0.2 M ABS (pH 5) and the scan rates are varied from 50 mV/s to 175 mV/s.

Nanotube deposition on a bare electrode surface influences the peak-to-peak potential separation. The responses of bare planar and porous modified electrodes are experimentally validated, as shown in Fig. 7A, where a GCE modified with 1.5 μg MWCNT has $\Delta E_{pp} = 0.040$ V compared to 0.066 V for the GCE. The influence of varying MWCNT mass, a surrogate for L , is investigated for different amounts of nanotube deposition on GCEs (Fig. 7B). As the MWCNT mass on the GCE increases from 1.5 μg , both the oxidation (A) and reduction (C_2) peaks shift to higher over-potentials, increasing peak-to-peak separation. For 4.5 μg of MWCNT and up, the peak-to-peak separation reaches that of the GCE ($\Delta E_{pp} = 0.066$ V). That ΔE_{pp} saturates after a sufficiently large layer thickness is consistent with the simulation in Section 4.1. Hence, we induce that while thin-layer effects influence the FT electrochemical response of an MWCNT/GCE, the electrocatalytic property of the MWCNT remains unaltered.

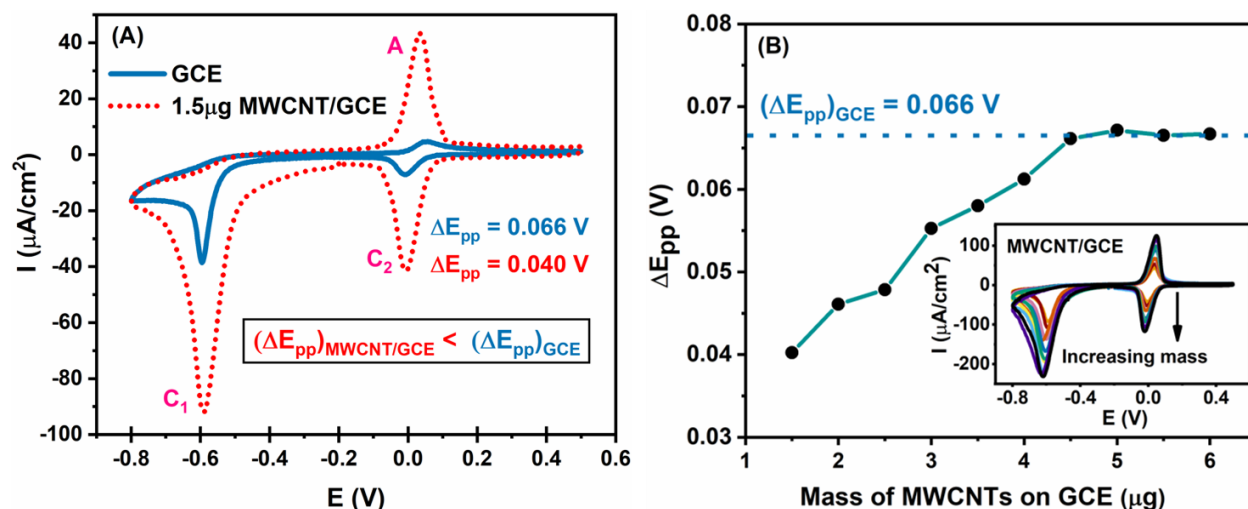


Figure 7. (A) Cyclic voltammograms showing peak-to-peak potential separations. The ΔE_{pp} responses of the GCE and MWCNT/GCE are compared for 1 mM FT. (B) Variation of ΔE_{pp} with respect to the MWCNT mass deposited on a GCE for 1 mM FT. The inset represents cyclic voltammograms for increasing MWCNT mass on a GCE for 1 mM FT. The scan rate is 50 mV/s.

Conclusions

MWCNT are deposited on GCE to modify planar electrodes to detect Fenitrothion (FT), an organophosphate (OP). We hypothesize that, as the thickness of the deposited MWCNT layer decreases, FT mass transport between the layers of porous multiwalled carbon nanotubes changes from semi-infinite to thin-layer diffusion. This influences the electrode electrochemical response to the analyte. Using simulations and experiments, we demonstrate thin-layer effects during FT detection by an MWCNT/GCE. These effects alter FT mass transport and influence the electrode electrochemical response to this chemical species. The change in FT diffusion as the deposition layer thickness decreases reduces the peak-to-peak potential separation during cyclic voltammetry. Simulations of the CV response of an electrode to FT are conducted with both the semi-infinite and thin-layer diffusion models for the planar (GCE) and modified porous (MWCNT/GCE) electrodes. We show that, along with the contribution of altered electrocatalysis, changes in FT diffusion should also be considered to understand the electrochemical response of nanotube-

modified electrodes. The model is applicable for other toxic chemicals like 4-nitrophenol, parathion and methyl parathion.

Acknowledgements

This work was supported by the Natural Sciences and Engineering Research Council of Canada (NSERC) Discovery Grant (RGPIN-2019-06571). The authors thank Dr. Carmen Andrei of Canadian Centre for Electron Microscopy for TEM.

5. References

- (1) Mulchandani, A.; Chen, W.; Mulchandani, P.; Wang, J.; Rogers, K. R. Biosensors for direct determination of organophosphate pesticides. *Biosensors and Bioelectronics* **2001**, *16* (4), 225-230. DOI: [https://doi.org/10.1016/S0956-5663\(01\)00126-9](https://doi.org/10.1016/S0956-5663(01)00126-9). Parham, H.; Rahbar, N. Square wave voltammetric determination of methyl parathion using ZrO₂-nanoparticles modified carbon paste electrode. *Journal of Hazardous Materials* **2010**, *177* (1), 1077-1084. DOI: <https://doi.org/10.1016/j.jhazmat.2010.01.031>.
- (2) Liu, G.; Lin, Y. Electrochemical Sensor for Organophosphate Pesticides and Nerve Agents Using Zirconia Nanoparticles as Selective Sorbents. *Analytical Chemistry* **2005**, *77* (18), 5894-5901. DOI: 10.1021/ac050791t.
- (3) Pimentel, D. Environmental and economic costs of the application of pesticides primarily in the United States. *Environment, development and sustainability* **2005**, *7* (2), 229-252.
- (4) Sherma, J.; Zweig, G. Pesticides. *Analytical chemistry* **1985**, *57* (5), 1-15.
- (5) Tuan, S.-J.; Tsai, H.-M.; Hsu, S.-M.; Li, H.-P. Multiresidue analysis of 176 pesticides and metabolites in pre-harvested fruits and vegetables for ensuring food safety by gas chromatography and high performance liquid chromatography. *Journal of Food and Drug Analysis* **2009**, *17* (3).
- (6) Du, D.; Ye, X.; Zhang, J.; Liu, D. Cathodic electrochemical analysis of methyl parathion at bismuth-film-modified glassy carbon electrode. *Electrochimica Acta* **2008**, *53* (13), 4478-4484. DOI: <https://doi.org/10.1016/j.electacta.2008.01.023>.
- (7) Fan, S.; Xiao, F.; Liu, L.; Zhao, F.; Zeng, B. Sensitive voltammetric response of methylparathion on single-walled carbon nanotube paste coated electrodes using ionic liquid as binder. *Sensors and Actuators B: Chemical* **2008**, *132* (1), 34-39.
- (8) Canevari, T. C.; Prado, T. M.; Cincotto, F. H.; Machado, S. A. Immobilization of ruthenium phthalocyanine on silica-coated multi-wall partially oriented carbon nanotubes: electrochemical detection of fenitrothion pesticide. *Materials Research Bulletin* **2016**, *76*, 41-47. Khan, I.; Pandit, U. J.; Wankar, S.; Das, R.; Limaye, S. N. Fabrication of electrochemical nanosensor based on polyaniline film-coated AgNP-MWCNT-modified GCE and its application for trace analysis of fenitrothion. *Ionics* **2017**, *23* (5), 1293-1308.
- (9) Streeter, I.; Wildgoose, G. G.; Shao, L.; Compton, R. G. Cyclic voltammetry on electrode surfaces covered with porous layers: an analysis of electron transfer kinetics at single-walled carbon nanotube modified electrodes. *Sensors and Actuators B: Chemical* **2008**, *133* (2), 462-466.
- (10) Jangid, K.; Sahu, R. P.; Pandey, R.; Chen, R.; Zhitomirsky, I.; Puri, I. K. Multiwalled Carbon Nanotubes Coated with Nitrogen-Sulfur Co-Doped Activated Carbon for Detecting Fenitrothion. *ACS Applied Nano Materials* **2021**, *4* (5), 4781-4789. DOI: 10.1021/acsnm.1c00376.
- (11) Tefera, M.; Admassie, S.; Tessema, M.; Mehretie, S. Electrochemical sensor for determination of fenitrothion at multi-wall carbon nanotubes modified glassy carbon electrode. *Analytical and Bioanalytical Chemistry Research* **2015**, *2* (2), 139-150.
- (12) Salehzadeh, H.; Ebrahimi, M.; Nematollahi, D.; Salarian, A. A. Electrochemical study of fenitrothion and bifenox and their simultaneous determination using multiwalled carbon nanotube modified glassy carbon electrode. *Journal of Electroanalytical Chemistry* **2016**, *767*, 188-194.
- (13) Sims, M. J.; Rees, N. V.; Dickinson, E. J.; Compton, R. G. Effects of thin-layer diffusion in the electrochemical detection of nicotine on basal plane pyrolytic graphite (BPPG) electrodes modified with layers of multi-walled carbon nanotubes (MWCNT-BPPG). *Sensors and Actuators B: Chemical* **2010**, *144* (1), 153-158.

- (14) Henstridge, M. C.; Dickinson, E. J.; Aslanoglu, M.; Batchelor-McAuley, C.; Compton, R. G. Voltammetric selectivity conferred by the modification of electrodes using conductive porous layers or films: the oxidation of dopamine on glassy carbon electrodes modified with multiwalled carbon nanotubes. *Sensors and Actuators B: Chemical* **2010**, *145* (1), 417-427.
- (15) Keeley, G. P.; Lyons, M. E. The effects of thin layer diffusion at glassy carbon electrodes modified with porous films of single-walled carbon nanotubes. *Int. J. Electrochem. Sci* **2009**, *4*, 794-809. Kätelhön, E.; Compton, R. G. Unscrambling illusionary catalysis in three-dimensional particle-modified electrodes: Reversible reactions at conducting particles. *Applied Materials Today* **2020**, *18*, 100514.
- (16) Yin, H.; Zhou, Y.; Ai, S.; Liu, X.; Zhu, L.; Lu, L. Electrochemical oxidative determination of 4-nitrophenol based on a glassy carbon electrode modified with a hydroxyapatite nanopowder. *Microchimica acta* **2010**, *169* (1-2), 87-92. Piovesan, J. V.; Haddad, V. F.; Pereira, D. F.; Spinelli, A. Magnetite nanoparticles/chitosan-modified glassy carbon electrode for non-enzymatic detection of the endocrine disruptor parathion by cathodic square-wave voltammetry. *Journal of Electroanalytical Chemistry* **2018**, *823*, 617-623.
- (17) Shams, N.; Lim, H. N.; Hajian, R.; Yusof, N. A.; Abdullah, J.; Sulaiman, Y.; Ibrahim, I.; Huang, N. M. Electrochemical sensor based on gold nanoparticles/ethylenediamine-reduced graphene oxide for trace determination of fenitrothion in water. *RSC advances* **2016**, *6* (92), 89430-89439.
- (18) Compton, R. G.; Katelhon, E.; Ward, K. R.; Laborda, E. *Understanding voltammetry: simulation of electrode processes*; World Scientific, 2020.
- (19) Batchelor- McAuley, C.; Li, D.; Compton, R. G. Mass- Transport- Corrected Transfer Coefficients: A Fully General Approach. *ChemElectroChem* **2020**, *7* (18), 3844-3851. Guidelli, R.; Compton, R. G.; Feliu, J. M.; Gileadi, E.; Lipkowski, J.; Schmickler, W.; Trasatti, S. Definition of the transfer coefficient in electrochemistry (IUPAC Recommendations 2014). *Pure and Applied Chemistry* **2014**, *86* (2), 259-262. Guidelli, R.; Compton, R. G.; Feliu, J. M.; Gileadi, E.; Lipkowski, J.; Schmickler, W.; Trasatti, S. Defining the transfer coefficient in electrochemistry: An assessment (IUPAC Technical Report). *Pure and Applied Chemistry* **2014**, *86* (2), 245-258.
- (20) Bard, A. J.; Faulkner, L. R. Fundamentals and applications. *Electrochemical methods* **2001**, *2* (482), 580-632.